Journal of Power Sources 196 (2011) 9780–9785

Contents lists available at ScienceDirect

Journal of Power Sources

journal homepage: www.elsevier.com/locate/jpowsour

Nanocone-arrays supported tin-based anode materials for lithium-ion battery

Zhijia Du, Shichao Zhang*, Yalan Xing, Xiaomeng Wu

School of Materials Science and Engineering, Beihang University, XueYuan Road No. 37, HaiDian District, Beijing 100191, PR China

ARTICLE INFO

Article history:
Received 5 April 2011
Received in revised form 24 June 2011
Accepted 2 August 2011
Available online 9 August 2011

Keywords:
Nanocone-arrays
Nanostructure
Tin
Lithium-ion battery

ABSTRACT

The electrodeposited nickel nanocone-arrays without any template are introduced to Sn-based anode materials as current collector for lithium ion battery. Nickel nanocone-arrays are tightly wedged in the electrodeposited Sn film, and thereby enhance the interfacial strength between active materials and substrate. Furthermore, annealing is conducted to form Sn–Ni alloy, in which Ni renders an inactive matrix to buffer volume change during cyclic lithiation/delithiation. The nanocone-arrays supported Sn–Ni alloy anode shows satisfactory Li^+ storage properties with the first reversible capacity of 807 mAh g^{-1}. The charge capacity for the 50th cycle is 678 mAh g^{-1}, delivering good retention rate of 99.6% per cycle. These improved performances of nickel nanocone-arrays supported Sn–Ni alloy anodes indicate the potential of their application as electrode materials for high performance energy storage.

© 2011 Elsevier B.V. All rights reserved.

1. Introduction

The demand for high capacity, long life Li-ion battery has been steadily increasing for future power tools, such as portable electronics and electric/hybrid vehicles [1,2]. Tin has been targeted to replace carbon as one of the most promising negative electrodes owing to its high intrinsic capacity of 994 mAh g^{-1}, which received extensive research efforts [3,4]. However, severe volume expansion occurred in tin electrode due to lithiation/delithiation process during charge–discharge cycles, which induced severe pulverization and shedding from the current collector [3,5]. This mechanical disintegration and electronic degradation thereby triggered drastic capacity fading and hindered its practical implementation.

To circumvent these issues, one efficient way is to design specific structured substrate with high roughness to improve adhesive properties between active materials and current collector. Tamura et al. demonstrated that a rough surface Cu foil efficiently improved the cycle performance of a Sn-based anode [6,7]. Kwon et al. introduced a nodule-type Cu substrate for electrodeposited Sn–Ni alloy, which noticeably increased the capacity and cyclic properties of Sn–Ni alloy electrode in the first 25 cycles [8]. Simon et al. and Scrosati et al. devoted large research efforts to optimizing the electrode configurations and obtained a series of remarkable achievements in lithium ion battery anodes [9–11]. However, this method has some disadvantages such as comparatively complicated procedures and high synthesis costs.

Another promising strategy is that of turning to Sn-based intermetallics to decrease the volume changes and obtain good electrochemical properties. The principal concept in the use of Sn-based intermetallics rather than pure tin is that, Sn and Li form the desired Li_xSn alloy in charge process while the other metal functions as an electrochemically inactive matrix to buffer the volume expansion during the alloying process [3]. In previous researches, various transition metals have been recommended as the inactive components in Sn-based intermetallics to achieve the improvement of lithium storage performance but only to a limited extent [12–18].

Recently, we have developed an innovative electrode design composed of nickel nanocone-arrays current collectors covered with silicon coatings via a convenient and economical two-step process: electrodeposition and radiofrequency sputtering [19]. Compared with silicon, tin possesses more advantages: low cost in preparation procedure, comparable high packing density, high conductivity, the safe lithiation potential at ~1.0 to ~0.3 V, no suffering from solvent cointercalation, etc.

In this paper, we report results obtained with nickel nanocone-arrays covered with Sn-based materials and prove their significant improvement of electrochemical properties in lithium-ion batteries. The design includes well-aligned nickel nanocones which make the surface roughness of the substrates from the previous reported micro-scale to nano-scale for the first time. Accordingly, the nickel nanocone-arrays function as the inactive confining buffer to accommodate the volume variation as well as the structural support to enhance the adhesion strength between the active materials and current collectors. Tin is electrodeposited on the substrates and subsequently annealed to form the Sn–Ni alloy phase which is thought can further alleviate the internal stress induced by volumetric change in cycling. The nickel nanocone-arrays supported

* Corresponding author. Tel.: +86 10 82338148; fax: +86 01 82339319.
E-mail address: csc@buaa.edu.cn (S. Zhang).

0378-7753/$ – see front matter © 2011 Elsevier B.V. All rights reserved.
doi:10.1016/j.jpowsour.2011.08.012

Sn-based anodes exhibit relatively high reversible capacity of >600 mAh g^{-1} with 76% retention rate over a prolonged 70 cycles.

2. Experimental

Nickel nanocone-arrays were obtained by the oriented electrocrystallization method [20]. A 99.9% Ni plate was used as the anodic electrode while a copper foil with thickness of ~14 μm was employed as the cathodic electrode for Ni nanocone-arrays deposition. The electrodeposition solution was composed of analytical pure $NiCl_2{\cdot}6H_2O$ 1 mol L^{-1}, H_3BO_3 0.5 mol L^{-1}, and ethylenediamine dihydrochloride 1.8 mol L^{-1} dissolved in deionized water. The temperature of deposition solution was maintained at 60 °C. The deposition current density was 15 mA cm^{-2} with deposition time of 5 min. After deposition, the samples were rinsed with deionized water for three times and then dried in vacuum at 60 °C.

The electrodes were prepared by electrodepositing tin onto Ni nanocone-arrays. The electrolytic bath consisted of analytical pure $SnSO_4$ 0.15 mol L^{-1}, H_2SO_4 (98%) 1.5 mol L^{-1}, polyethylene glycol (PEG) 10 mL·L^{-1} and bis-(sodium sulfopropyl)-disulfide (SPS) 10 mL L^{-1}. Tin plate was used as anode and the electrolytic solution was continually agitated by a magnetic bar. The deposition was conducted under pulsed current of −20 mA cm^{-2} for 600 s, whose frequency is 10 Hz with an on/off ratio waveform of 1:9. The working temperature of both steps was 25 °C. After Sn deposition, the obtained anodes were washed with distilled water and acetone successively and then dried at 60 °C under argon atmosphere. The annealing was conducted at 210 °C for 5 h in vacuum to produce Sn–Ni alloy electrodes. The mass of the as-prepared Sn deposit was calculated by measuring the Ni nanocone-arrays substrate before and after the electrodeposition via a METTLER AB135-S analytical balance with accuracy of 0.01 mg. For convenient comparison of the as-deposited and annealed electrodes, the gravimetric capacity was calculated by dividing the amount of charges by the measured weight, thereby representing only the capacity of Sn.

The morphologies, element distribution and phase structure of the electrodes were investigated by field emission scanning electron microscopy (FE-SEM, Hitachi S-4800 SEM system), its adjunctive energy dispersive X-ray spectroscope (EDS) and MAC Science X-ray diffraction (Cu Kα radiation), respectively.

Electrochemical charge–discharge behaviors were investigated in stimulant cells assembled with the as-prepared anode, lithium foil and Celgard 2300 membrane in an Ar filled glove box (MB-10-G with TP170b/mono, MBRAUN). 1 M $LiPF_6$/EC-DEC (1:1 by vol.) was used as the electrolyte. Each cell was aged for 20 h at room temperature before commencing the electrochemical tests. The galvanostatic charge–discharge measurements were carried out in a battery test system (NEWARE BTS-610, Newware Technology Co., Ltd., China) at room temperature. The cut-off voltage for 0.2 C rate tests was 0.05–1.5 V.

3. Results and discussion

Fig. 1 shows a typical scanning electron microscopy (SEM) image of the nickel nanocone-arrays. It can be concluded from the figures that most of the nanocones grew vertically to the substrates. The average height of the cones and the mean diameter of their roots are approximately 400 nm and 180 nm, respectively. The tips of the cones are very sharp, corresponding to an apex angle of ~29°. The arrays density of the cones is calculated to be about 2×10^{10} cones cm^{-2}. The growth process of the nickel nanocone-arrays was template-free, which was somewhat different from the traditional arrays growth method with ordered templates such as AAO [10]. Therefore, the nickel cones are not very regular and uniform. Slightly tilted, larger and smaller cones are also observed in the mix.

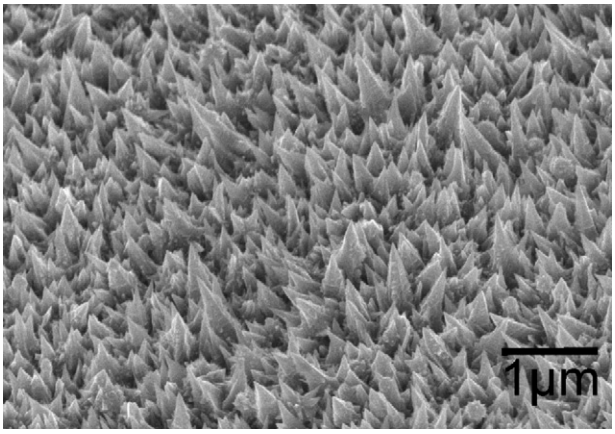

Fig. 1. SEM image of electrodeposited Ni nanocone-arrays.

With the supporting substrate which surface roughness was nano-scale constructed, electrodepostion of tin on these cones was carried out afterwards to produce the electrode. Top view in Fig. 2a shows that the morphology of the as-deposited electrode is composed of a contiguous film with serried protuberances upside, which probably inherited from the bottom nickel nanocones. High magnification image in the inset of Fig. 2a clearly manifests that the size of tin particles in the deposit is dozens of nanometers. Tin deposition was performed by two different pulsed current step conditions: Step 1 was a cathodic current pulse of −20 mA cm^{-2} lasting 10 ms while Step 2 was 90 ms of rest (i.e. open circuit). As a result, tin nucleation and growth was confined to the time of every 10 ms, thereby obtaining nano-scaled particles. Besides, an EDS line scan (along the red line in Fig. 2b) across the sectional surface of as-deposited tin electrode was performed to confirm the element distribution. The EDS data clearly show that Sn is located in the surface layer with thickness of ~1.5 μm, Ni is in the interlayer while Cu is in the basal-layer. This is consistent with the schematic diagram illustrating the fabrication of Ni nanocone-array supported Sn anode architecture as shown in the inset of Fig. 2b. (For interpretation of the references to color in this text, the reader is referred to the web version of the article.)

Previous researches reported that the adhesion strength can be enhanced by annealing [21], Therefore, annealing was applied to accomplish the maximal binding force between active materials and substrate, which would also produce the desired Sn–Ni intermetallic. Compared to the pristine sample in Fig. 2a, the morphology of annealed electrode in Fig. 2c suggests apparently less change. Nevertheless, the surface undulation was less obvious and the particles boundary was less distinct as shown in Fig. 2c and its inset. In light of this variation, new phase was thought to be formed on the surface of the Sn-based anode by the annealing for 5 h. Furthermore, an EDS line scan (along the red line in Fig. 2d) across the sectional surface of the annealed electrode was also carried out. Basically, there was no evident variation in the Ni interlayer and Cu basal-layer. However, compared to the as-deposited tin electrode, Ni elemental signal enhanced in the surface layer of the annealed electrode, which suggested Ni had diffused to the surface layer in the annealing process.

To directly confirm whether the phase had changed in the electrode, X-ray diffraction (XRD) measurement was performed for the as-deposited electrode and the annealed electrode as shown in Fig. 3. The XRD pattern of as-deposited electrode shows the peaks of the Cu substrate, Ni interlayer and small amount of β-Sn. After

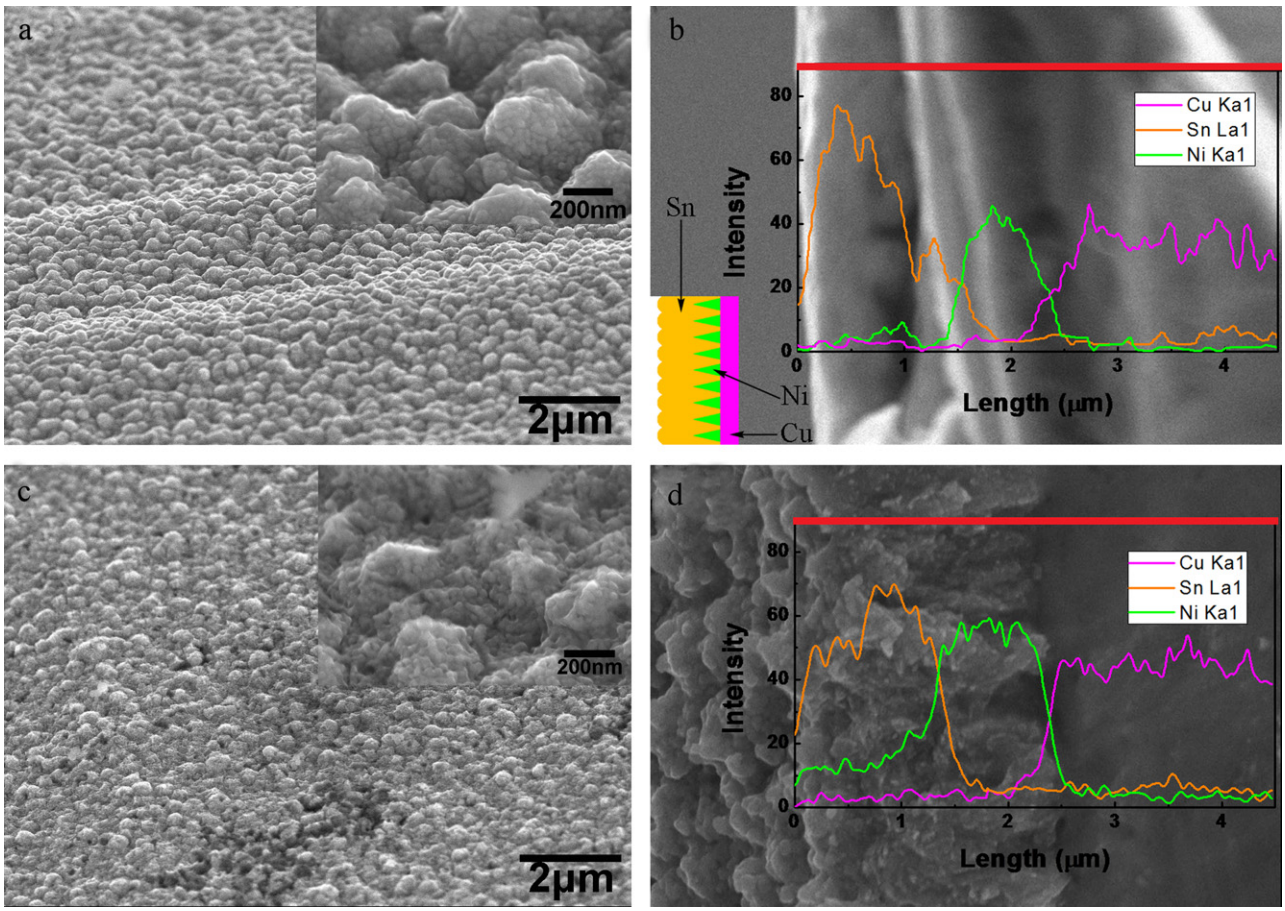

Fig. 2. SEM images on the surface morphology of Ni nanocone-arrays supported electrode: (a and its inset) as-deposited Sn electrode; (b) EDS line scan across the sectional surface of as-deposited Sn electrode, the inset is the schematic diagram of Ni nanocone-array supported Sn anode architecture; (c and its inset) SEM images of annealed Sn-based electrode; (d) EDS line scan across the sectional surface of the annealed electrode.

annealing, however, the β-Sn phase disappeared with the evolution of Ni_3Sn_4 intermetallic phase. This result can be simply attributed to the diffusion of Ni from the substrate into the electrode and its reaction with Sn. This difference in phase is quite convenient for comparing the electrochemical behavior of the nanostructured Sn–Ni intermetallic electrode versus that of the nanostructured pure Sn electrode, which will be discussed later.

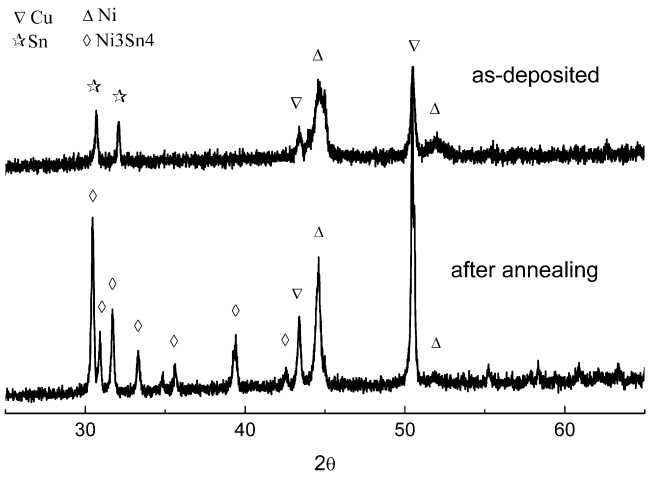

Fig. 3. XRD patterns of the as-deposited Sn anode and the Sn-based anode after annealing at 210 °C for 5 h.

After the deposition of tin and its annealing, the Ni nanocone-arrays functioned directly as current collectors and tin or Ni_3Sn_4 alloy acted as the active material so that the exclusion of binder and conductive agents would prevent some undesirable phenomena such as the isolation of Li^+ as reported before [8]. The two kinds of samples were directly assembled into half-cells with Li metal as the counter electrode to investigate their Li-storage properties. Fig. 4a and b shows the voltage profiles generated by the as-deposited tin and annealed Ni_3Sn_4 alloy electrodes at a current density of 198 mA g^{-1} (rate = 0.2 C), respectively. From the voltage profile in Fig. 4a, it can be seen that the electrochemical lithiation and delithiation of the as-deposited tin is consistent with previous reports on pure Sn anodes [4]. Three plateaus are observed during discharge at ~0.66 V, ~0.49 V and ~0.38 V corresponding to lithiation potential of Sn, Li_2Sn_5 and LiSn. The following sloping region gradually dropping to 0.01 V is related to further lithiation of Sn to form successive lithium-rich phases Li_xSn_y. There is a noticeable irreversible capacity corresponding to the sloping curve above 0.66 V, which is induced by the formation of SEI (solid electrolyte interphase) layer and/or the reduction of possible oxide impurities on electrode surface [12]. Several plateaus are also observed during charge as a consequence of lithium extraction from a series of Li_xSn_y alloys. The discharge–charge profiles for the 2nd and 5th cycles coincide, which indicates a stable electrochemical performance of the nickel nanocone-arrays supported Sn electrode.

However, the voltage profile of Ni_3Sn_4 electrode in Fig. 4b is very different from the as-deposited one. The active/inactive structure of Ni_3Sn_4 intermetallic electrode produced a potential profile (shown in Fig. 4b) lacking the plateaus that are characteristic of

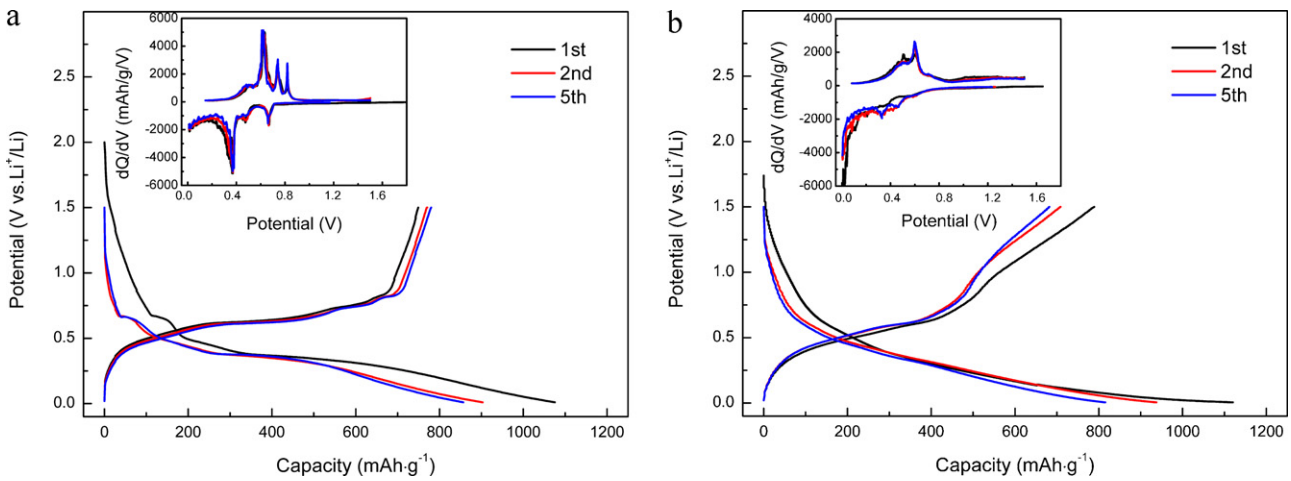

Fig. 4. Voltage profiles and differential capacity with potential (the insets) of the electrodes cycled between 10 mV and 1.5 V at 0.2 C rate: (a) as-deposited Sn anode and (b) annealed Ni_3Sn_4 anode.

lithium insertion into the different Li_xSn_y phases. It is considered that Sn metal cluster is hardly formed in the electrode owing to the existence of inactive Ni matrix during the discharge/charge cycles [13]. Actually, the smoother profile in Ni_3Sn_4 alloy case is more appropriate for the estimation of SOC (state of charge) which provides an indication of how much longer a battery will continue to perform before it needs recharging. After the first cycle, the discharge–charge profiles overlapped as well, which suggests the Sn–Ni alloy electrode similarly has the steady Li^+ storage properties.

The plots of differential capacity with potential for the nickel nanocone-arrays supported Sn and Ni_3Sn_4 electrode are inset in Fig. 4a and b, respectively. In contrast with the fine and sharp peaks in the pure Sn anode as a consequence of lithiation/delithiation of the certain Li_xSn_y, the curve of Ni_3Sn_4 anode is featureless and very broad. The broad characteristics of the differential capacity curve are indicative of no aggregation of Sn atoms to react with lithium [22,23].

Fig. 5 depicts the reversible capacity versus cycle number plots at a discharge/charge rate of 0.2 C, providing a direct evidence of the good lithium storage performance due to the introduction of nickel nanocone-arrays substrate into Sn-based electrode. For the as-deposited Sn anode, the first charge capacity is 757 mAh g^{-1}, which is approximately twice that of commercial graphite. The capacity for the 30th cycle is 628 mAh g^{-1} with retention rate of

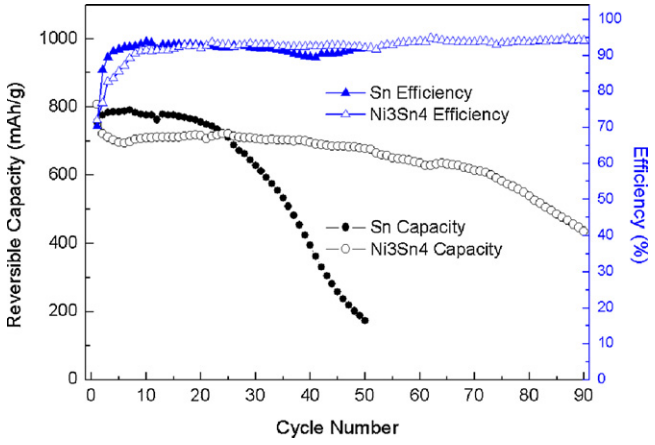

Fig. 5. Reversible capacity and Coulombic efficiency versus cycle number for the as-deposited Sn anode and annealed Ni_3Sn_4 anode.

83%, indicating the cycling performance in the first 30 cycles is fairly good. Considering the Sn deposits are interlaced with the nickel nanocone-arrays, the enhanced binding strength between active materials and current collector is obtained by the mechanical interlocking effect. This improvement is considerably superior to the previous reported ones with micro-scale roughed copper foil [6,8], because the Ni cone-arrays which deeply wedged into Sn film also act somewhat as the confining buffer to accommodate the enormous volume variations and relieve the associated huge stresses owing to repeated Li alloying/dealloying with Sn. However, the charge capacity subsequently fades drastically to 174 mAh g^{-1}, leaving retention rate of only 23% after 50 cycles.

To obtain a better cyclability, annealing is chosen to form active/inactive Sn–Ni intermetallic electrode. Additionally, annealing can also strengthen the electrode–substrate adhesion as reported before [21]. Fig. 5 also exhibits the excellent cycling properties in prolonged cycles of nickel nanocone-arrays supported Ni_3Sn_4 electrode. The first charge capacity is 807 mAh g^{-1}, slightly larger than that of the as-deposited sample. Afterwards the reversible capacity maintained relatively stable. For example, the charge capacity for the 70th cycle was 614 mAh g^{-1}, corresponding to retention rate of 76%, or 99.6% per cycle. The evolution of Ni_3Sn_4 intermetallic from pure Sn firstly provides an inactive Ni matrix to buffer the volume expansion/contraction during repeat lithiation/delithiation. On the other hand, the mechanical interlocking caused by nickel nanocone-arrays as well as the atomic interdiffusion induced by annealing renders a good adhesion between the active materials and the substrate so that they maintain contact during volume variations thereby increasing the cyclability. However, the capacity fades drastically after the 70th cycle. The charge capacity is 435 mAh g^{-1} after 90 cycles with retention rate of only 54%.

To determine whether the morphology of nanocone-arrays supported Sn and Ni_3Sn_4 electrode had changed after repeated lithium alloying/dealloying, the cells was disassembled after the given cycles for SEM characterization of the electrodes as shown in Fig. 6a–c. Cracking of the Sn film is first revealed after 30 cycles (not shown). Finally, pulverization and exfoliation of the Sn film are observed all over the current collector after the 50th cycle (in Fig. 6a). This would be regarded as the main cause of the capacity decrease.

Contrarily, the morphology of Ni_3Sn_4 electrode after 50 cycles (Fig. 6b) shows less variation compared to the image of the pristine sample (Fig. 2c). Considering the Ni_3Sn_4 intermetallic offers an inactive Ni matrix, the enormous volume change and internal strain

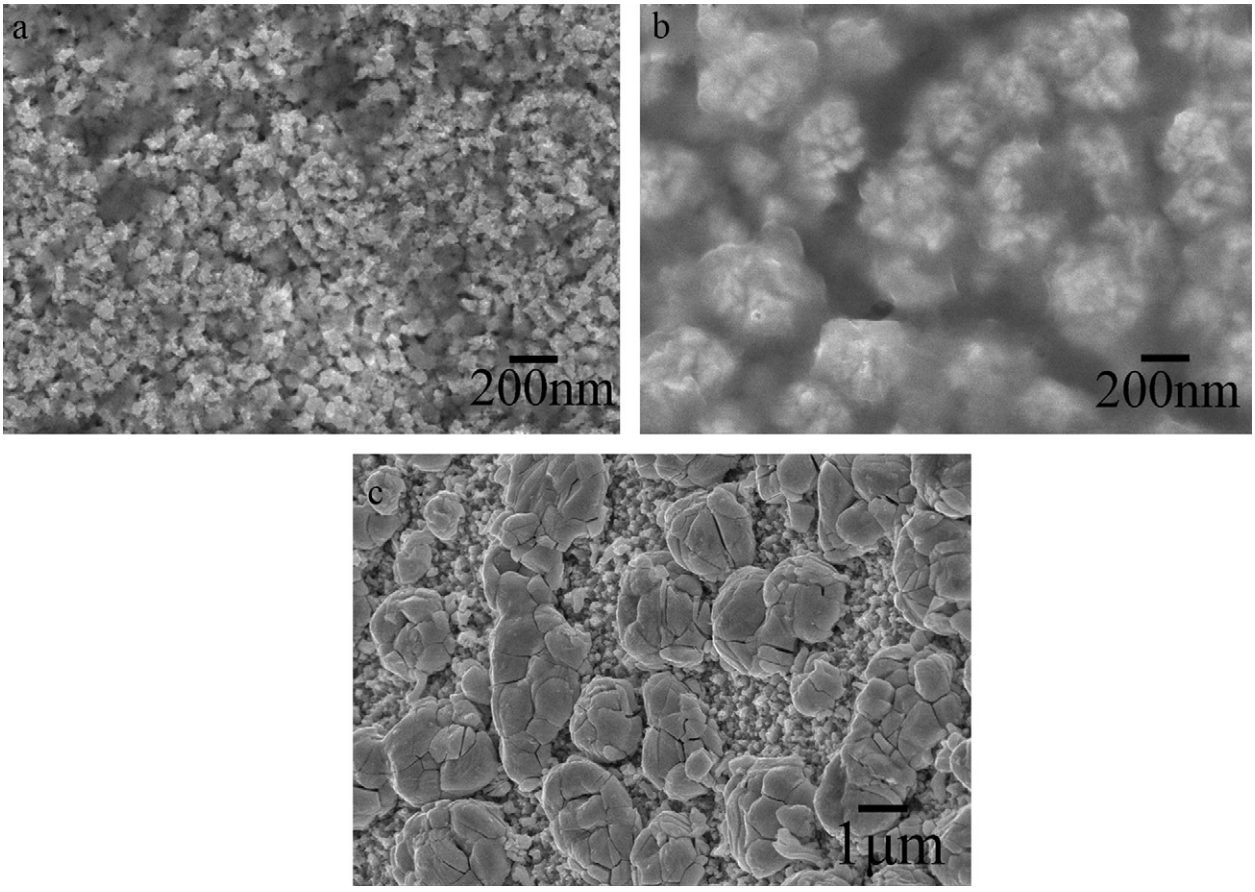

Fig. 6. SEM images of (a) as-deposited Sn anode after 50 cycles, (b) annealed Ni_3Sn_4 anode after 50 cycles and (c) annealed Ni_3Sn_4 anode after 90 cycles.

are accommodated to avoid cracking. Eventually, the annealed film has not disintegrated and degraded with the Ni nanocone-arrays sticking to the active materials tightly. This proves the advantage of our well-designed nickel nanocone-arrays supported Ni_3Sn_4 electrodes over previous reported Sn-based electrode with micro-scaled nodule-type substrate, in which the capacity retention rate for the first 25 cycles was improved to approximately 66% [8]. The morphology of Ni_3Sn_4 electrode after 90 cycles is shown in Fig. 6c to make clear the reason for fierce capacity fading in 70th to 90th cycles. Agglomeration and cracking are observed on the surface of the electrode. This is probably because the formation of Ni_3Sn_4 phase in the annealing process consumed some Ni atoms in the nickel cones thereby decreasing the mechanical interlocking effect, especially after many periodic volume variations. Therefore, there is still room for cycle performance improvement by, for example, increasing the cones height and directly depositing Sn-based alloys.

4. Conclusions

In summary, nickel nanocone-arrays supported Sn-based film was synthesized as the anode material for Li-ion batteries. In this electrode, nickel nanocone-arrays serves as current collector to enhance the binding force between the active materials and substrate and relieve the huge interfacial strains induced by volume expansion. The as-deposited Sn anode showed improvement in cycling performance in the first 30 cycles, which followed by a rapid capacity fading. Therefore, annealing was conducted for the formation of Ni_3Sn_4 alloy, in which the inactive Ni acts as a buffer matrix to accommodate the volume variation generated by repeat lithiation/delithiation. The nanocone-arrays supported Ni_3Sn_4 anode exhibited impressive lithium storage capability at 0.2 C rate. The reversible capacity for the first cycle was 807 mAh g^{-1}, and for the 70th cycle that was 614 mAh g^{-1} with superior retention of 99.6% per cycle. The proposed approach with a very facile procedure may be also exploited for other active materials to achieve a high-capacity and durable electrode for Li-ion batteries.

Acknowledgements

This work was supported by the National Natural Science Foundation of China (50954005, 51074011), National Basic Research Program of China (2007CB936502) and National 863 Program (2006AA03Z230 and 2008AA03Z208), and the Innovation Foundation of BUAA for PhD Graduates as well as the Scholarship Award for Excellent Doctoral Student granted by China Ministry of Education.

References

[1] J.B. Goodenough, Y. Kim, Chem. Mater. 22 (2010) 587.
[2] M. Armand, J.-M. Tarascon, Nature 451 (2008) 652.
[3] M. Winter, J.O. Besenhard, Electrochim. Acta 45 (1999) 31.
[4] I.A. Courtney, J.S. Tse, O. Mao, J. Hafner, J.R. Dahn, Phys. Rev. B 58 (1998) 15583.
[5] L.Y. Beaulieu, S.D. Beattie, T.D. Hatchard, J.R. Dahn, J. Electrochem. Soc. 150 (2003) A419.
[6] N. Tamura, R. Ohshita, M. Fujimoto, M. Kamino, S. Fujitani, J. Electrochem. Soc. 150 (2003) A679.
[7] N. Tamura, M. Fujimoto, M. Kamino, S. Fujitani, Electrochim. Acta 49 (2004) 1949.
[8] N.-R. Shin, Y.-M. Kang, M.-S. Song, D.-Y. Kim, H.-S. Kwon, J. Power Sources 186 (2009) 201.
[9] P.L. Taberna, S. Mitra, P. Poizot, P. Simon, J.-M. Tarascon, Nat. Mater. 5 (2006) 567.

[10] J. Hassoun, S. Panero, P. Simon, P.L. Taberna, B. Scrosati, Adv. Mater. 19 (2007) 1632.
[11] L. Bazin, S. Mitra, P.L. Taberna, P. Poizot, M. Gressier, M.J. Menu, A. Barnabé, P. Simon, J.-M. Tarascon, J. Power Sources 188 (2009) 578.
[12] A.D.W. Todd, R.E. Mar, J.R. Dahn, J. Electrochem. Soc. 153 (2006) A1998.
[13] A.D.W. Todd, P.P. Ferguson, M.D. Fleischauer, J.R. Dahn, Int. J. Energy Res. 34 (2010) 535.
[14] J. Hassoun, S. Panero, B. Scrosati, J. Power Sources 160 (2006) 1336.
[15] V. Sivasankaran, C. Marino, M. Chamas, P. Soudan, D. Guyomard, J.C. Jumas, P.E. Lippens, L. Monconduit, B. Lestriez, J. Mater. Chem. 21 (2011) 5076.
[16] W. Pu, X. He, J. Ren, C. Wan, C. Jiang, Electrochim. Acta 50 (2005) 4140.
[17] P.A. Connor, J.T.S. Irvine, Electrochim. Acta 47 (2002) 2885.
[18] S.H. Ju, H.C. Jang, Y.C. Kang, J. Power Sources 189 (2009) 163.
[19] S. Zhang, Z. Du, R. Lin, T. Jiang, G. Liu, X. Wu, D. Weng, Adv. Mater. 22 (2010) 5378.
[20] T. Hang, A. Hu, H. Ling, M. Li, D. Mao, Appl. Surf. Sci. 256 (2010) 2400.
[21] N. Tamura, R. Ohshita, M. Fujimoto, S. Fujitani, M. Kamino, I. Yonezu, J. Power Sources 107 (2002) 48.
[22] Y.-L. Kim, H.-Y. Lee, S.-W. Jang, S.-J. Lee, H.-K. Baik, Y.-S. Yoon, Y.-S. Park, S.-M. Lee, Solid State Ionics 160 (2003) 235.
[23] H.-Y. Lee, S.-W. Jang, S.-M. Lee, S.-J. Lee, H.-K. Baik, J. Power Sources 112 (2002) 8.